

Tight-binding Hamiltonian considering up to the third nearest neighbours for trans polyacetylene

M Ali M Keshtan  and Mahdi Esmailzadeh ¹ 

Department of Physics, Iran University of Science and Technology, Narmak, Tehran 16844, Iran

E-mail: m_ali_m_keshtan@physics.iust.ac.ir and mahdi@iust.ac.ir

Received 3 January 2020, revised 12 February 2020

Accepted for publication 10 March 2020

Published 15 April 2020



Abstract

Utilizing the linear combination of atomic orbitals in the Slater–Koster approach in combination with the density functional theory band structure data, a new tight-binding Hamiltonian up to the third nearest neighbours for the dimerized trans polyacetylene is proposed. The effects of strain are also considered in the Hamiltonian by varying the distance between two successive CH groups along the molecular symmetry axis. Using this new Hamiltonian and exploiting the Green’s function method in the framework of the Landauer–Büttiker formalism, the electronic transport properties in a trans polyacetylene chain in the presence and absence of strain are studied. It is shown that at a peculiar value of compression strain, the electron conductance shifts 0.27 eV in energy which is an exploitable magnitude for straintronic applications of the trans polyacetylene specially as strain sensors and strain switches.

Keywords: straintronics, Slater–Koster approach, Green’s function method, trans polyacetylene

 Supplementary material for this article is available [online](#)

(Some figures may appear in colour only in the online journal)

1. Introduction

Exploiting the material properties, persuades researchers in condensed matter and material physics to illustrate the responses of materials to all external interactions. ‘Straintronics’ is an infant branch of physics which was born by combining mechanical induced properties with electronic and spintronic properties of materials [1–3] to facilitate prompt enhancements of its nature, information and computation related technologies and devices [4, 5] especially in graphene and other 2D materials [6–10]. The next-generation electronic and spintronic devices must be lightweight, self-assembled, portable, wearable and even self-powered. Organic materials and molecules have played crucial roles in electronics and spintronics during the past three decades [11, 12].

The effects of interface [13] and optical properties in organic materials and molecules are well investigated [14, 15]. Besides, they are self-assembled and flexible [16–18]. These properties make them great candidates for the next-generation electronic and spintronic devices. Moreover, strain flexible sensors have been faced with a surge in demand for application during the past two decades [19]. As textile sensors, they must be flexible, stretchable, wearable, skin-mountable and weightless. Moreover they should incorporate the merits of cheapness, high sensitivity and feasibility of large-area fabrication [20]. These properties enable them to be utilized in electronic skins [21, 22], health care and sport monitoring devices [23], smart robots, artificial intelligence realms and human–machine interfaces for virtual reality even as entertainment [24].

As the first conducting polymer, polyacetylene was synthesized and has been studied well during the last four decades

¹ Author to whom any correspondence should be addressed.

[25–27]. Trans polyacetylene (TP) in its stable form [28], has attracted more attention and its electronic [29–31], mechanical [32, 33], optical [34, 35] and structural [36–39] properties have been investigated. Effects of defects on it were extensively studied [40, 41]. Saito and Kamimura calculated the vibronic states of TP [42] and Teramae and Yamabe investigated its geometrical structure [43]. Like other semi one dimensional systems, strain in TP was typically studied by considering the Peierls instability [44] as the pseudo magnetic phase or in the harmonic approximation [45–47].

In this work, the Slater–Koster (SK) approach [48] within the linear combination of atomic orbitals (LCAO) method is used to propose a new tight-binding (TB) Hamiltonian for the trans polyacetylene. Therefore, the SK coefficients are fitted to the density functional theory (DFT) band structure results. The celebrated Su–Schrieffer–Heeger (SSH) Hamiltonian includes just the first two nearest neighbours and π electrons (p_z orbitals) for hopping integrals with a band structure which is correct only near the Fermi energy [26] and possesses only two bands. However, this new model considers the third nearest neighbours and four s , p_x , p_y and p_z orbitals for finding the best results for the Hamiltonian entries and band structures which are well fitted to DFT generated band structures. Besides, the electronic transport properties of a TP wire are studied by exploiting the Green’s function method in the framework of the Landauer–Büttiker formalism. Furthermore, by varying the distance between two successive CH groups along the molecular symmetry axis and rewriting the Hamiltonian, the effects of compression and expansion strains are studied. It is found that the trans polyacetylene has a high strain sensitivity and this molecule can be considered as an adequate candidate for straintronic applications such as strain sensors and switches.

The rest of this paper is organized in this manner. In section 2 by using DFT calculation the ground state of the trans polyacetylene structure is found and its band structure is calculated. Then in section 3 a tight-binding Hamiltonian model is constructed by using band structure data. Effects of strain on the Hamiltonian and the charge conductance are illustrated and discussed in section 4 which is accompanied by a summary and outlook in section 5.

2. DFT electronic band structure

In this section, the electronic band structure properties of trans polyacetylene are determined by first-principles calculations with executing the OpenMx package [49]. The electronic band structure calculations besides the atomic structure relaxations are carried out within the linear combination of pseudo-atomic orbitals (LCPAO) method [50–52]². The exchange–correlation functional is included by the Perdew, Burke and Ernzerhof generalized gradient approximation [53, 54]. The plane-wave basis cutoff energy is set to 680

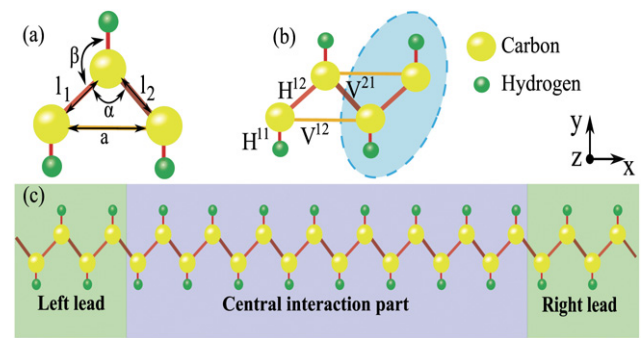


Figure 1. Schematic structure of a trans polyacetylene (a). The different parts of TB Hamiltonian describing a trans polyacetylene (b). A trans polyacetylene chain (c). The ellipse represents the unit cell.

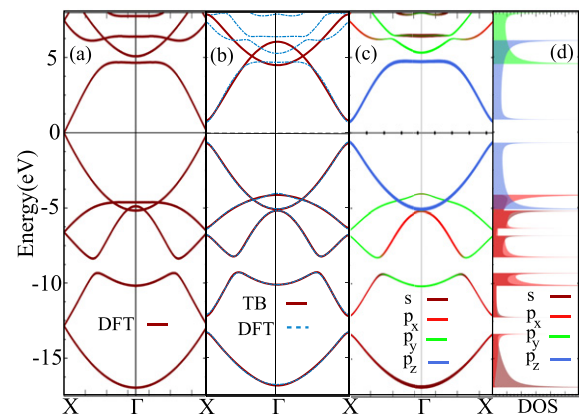


Figure 2. DFT band structure of the undimerized TP (a). DFT and TB band structures of a dimerized (b), the orbital resolved DFT band structure (c) and DOS for different orbitals calculated by TB Hamiltonian (d) for the dimerized TP.

eV and the structural relaxation force threshold considered to be 10^{-5} eV \AA^{-1} . The Brillouin zone grid with the Monkhorst–Pack mesh for the integration calculations is set to $12 \times 1 \times 1$.

The completely relaxed and optimized TP isomer is an undimerized structure with equidistant carbon–carbon bonding length $l_1 = l_2 = 1.393$ \AA , the carbon–carbon–carbon angle $\alpha = 124.2^\circ$, the carbon–carbon–hydrogen angle $\beta = 117.9^\circ$ and the lattice constant along the molecular symmetry axis $a = 2.466$ \AA (see figure 1(a)) which are in very good agreement with previous structural works [55, 56]. For the relaxed dimerized TP isomer the structure data become $l_1 = 1.33$ \AA , $l_2 = 1.48$ \AA , $\alpha = 124.2^\circ$, $\beta = 119.5^\circ$ and $a = 2.479$ \AA . The gapless metallic electronic band structure for the undimerized TP isomer is depicted in figure 2(a) while its semiconductor dimerized isomer electronic band structure is sketched in figure 2(b).

3. Tight-binding Hamiltonian model

Linear combination of atomic orbitals method is a celebrated tool to describe crystalline structures exploiting a set of non-interacting single particles. The SK approach has been vastly

² Using the standard library of OpenMx package, the atomic species for carbon atom are defined with ‘C7.0-s³p³d²’ and C PBE13’ while the atomic species for hydrogen atom are ‘H5.0-s³p²’ and H PBE13’.

utilized to establish the best TB Hamiltonian for solid state systems [57]. For the TP structure with two carbon atoms per unit cell (see figure 1(b)), ignoring the hydrogen atoms, four cubic harmonic orbitals s , p_x , p_y and p_z are considered per carbon atom [58]. In the general non-orthonormal case, the secular equation must be solved [59–61]. This equation can be written as

$$\sum_{\nu', i'} (H_{i\nu, i'\nu'} - \epsilon_k S_{i\nu, i'\nu'}) c_{i'\nu'}(k) = 0, \quad (1)$$

where

$$H_{i\nu, i'\nu'} = \langle \phi_{i\nu}(\mathbf{r} - \mathbf{r}_i) | H | \phi_{i'\nu'}(\mathbf{r} - \mathbf{r}_{i'}) \rangle, \quad (2)$$

$$S_{i\nu, i'\nu'} = \langle \phi_{i\nu}(\mathbf{r} - \mathbf{r}_i) | \phi_{i'\nu'}(\mathbf{r} - \mathbf{r}_{i'}) \rangle. \quad (3)$$

The single particle Hamiltonian is H and the overlap matrix is S while the basis set vectors are $\{\phi_{i\nu}\}$. In the case of orthonormal basis, the overlap matrix becomes an identity one. Dummies i and ν count all the atoms and their four orbitals s , p_x , p_y and p_z , in the unit cell and integrals are calculated over the real space unit cell. In the SK approach, the directional cosines are defined by $n_i = \frac{\mathbf{r} \cdot \mathbf{e}_i}{|\mathbf{r}|}$ where $i = x, y, z$ are the Cartesian directions and \mathbf{r} is a vector along the corresponding bond. The matrix entries represented by the expectation values of the Hamiltonian in the basis of the directed orbitals with eight integrals ($v_{ss\sigma}$, $v_{sp\sigma}$, $v_{pp\sigma}$, $v_{pp\pi}$, $s_{ss\sigma}$, $s_{sp\sigma}$, $s_{pp\sigma}$ and $s_{pp\pi}$) defined by

$$\begin{aligned} \langle s | H | s \rangle &= v_{ss\sigma}, \\ \langle s | H | p_i \rangle &= n_i v_{sp\sigma}, \\ \langle p_i | H | p_j \rangle &= n_i n_j v_{pp\sigma} + (\delta_{ij} - n_i n_j) v_{pp\pi}. \end{aligned} \quad (4)$$

Replacing H by S and v by s in equation (4), relations for overlap matrix are derived. Exploiting the directional cosines necessitates the usage of angular quantum number for calculation of the complex conjugate entries of the matrices ($\langle l | H | l' \rangle = (-1)^{l+l'} \langle l' | H | l \rangle$). The unidentified parameters must be clarified by fitting them to the known data, in this case, the DFT based band structures. Exploiting the typical Levenberg–Marquardt nonlinear fitting algorithm [62, 63], the most adequate entries for the Hamiltonian could be found. The basis can be chosen orthonormal for the dimerized TP isomer, hence only the Hamiltonian matrix entries must be calculated. Furthermore, in this model, to optimize the accuracy of calculations and their time and energy costs, due to the spatial distributions of effective orbitals and importance of all valence bands and the bands around the Fermi level, up to the third nearest neighbours are considered (see figures 1(a) and (b)). The SK coefficients are calculated by fitting DFT and TB Hamiltonian band structures which are depicted in figure 2(b) and are given in table 1. In figure 2(c) the orbital resolved DFT based band structure for the dimerized TP isomer is depicted. Also, the orbital resolved DOS diagram is plotted in figure 2(d) by using its TB Hamiltonian, which is in very good agreement with its corresponding DFT band structure which is depicted in figure 2(c).

As it is anticipated from comparison with the SSH model, p_z orbital plays the main role near the Fermi energy (see figure 3(b) gold curves and figure 2(c) sky blue curves).

Table 1. The Slater–Koster coefficients for the unstrained dimerized trans polyacetylene. All parameters are in eV.

R	$v_{ss\sigma}$	$v_{sp\sigma}$	$v_{pp\sigma}$	$v_{pp\pi}$
l_1	−2.796	0.409	−1.289	−3.188
l_2	−2.242	2.912	0.136	−2.421
A	−0.474	0.231	0.748	0.106

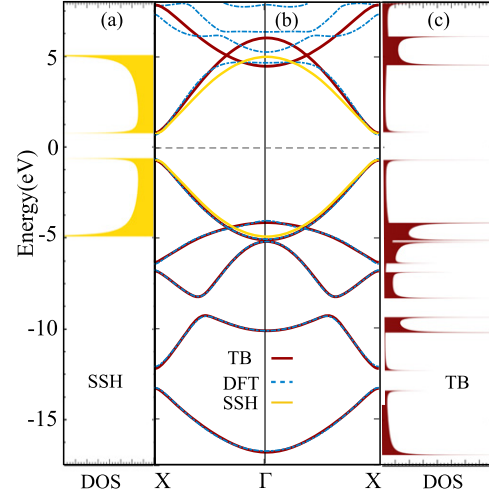


Figure 3. DFT, TB fitted and SSH model band structures of the dimerized unstrained trans polyacetylene (b). DOS for the SSH model (a) and DOS for the TB fitted (c) Hamiltonian.

Though the SSH model band structure behaves in good agreement with the other models near the Fermi energy, it can not describe phenomena far from the Fermi energy since it is not defined there. Comparison between DOS of the SSH model plotted in figure 3(a) and the TB fitted Hamiltonian depicted in figure 3(c) reveals this fact. Furthermore, the SSH model considers only two valence and conduction bands and therefore does not prognosticate behaviours related to other orbitals like band splitting induced by strain and its consequences (see figure 6).

Two distinct TB Hamiltonians for the dimerized TP with the third nearest neighbours model are obtained. The first one, H , describes the intra-unit cell interactions and the second one, V , explains the inter-unit cell interactions. Since there exist two carbon atoms in the unit cell and for each one, four orbitals are considered, both TB Hamiltonians for intra and inter-unit cell interactions are represented by 8×8 matrices with the general forms

$$H = \begin{pmatrix} H^{11} & H^{12} \\ H^{21} & H^{22} \end{pmatrix}; \quad V = \begin{pmatrix} V^{11} & V^{12} \\ V^{21} & V^{22} \end{pmatrix}, \quad (5)$$

where sub matrices, H^{ij} and V^{ij} with $i, j = 1, 2$ are 4×4 matrices with entries related to s , p_y , p_z and p_x orbitals, respectively. Therefore, each entry of main matrices is represented by H_{kl}^{ij} or V_{kl}^{ij} where $k, l = s, p_y, p_z$ and p_x . Symmetrical properties of the system impose many constraints on 64 entries of both Hamiltonians. For the intra-unit cell Hamiltonian, H , two diagonal sub Hamiltonians which describe carbon atoms are the same, i.e.,

Table 2. All nonzero entries of both intra and inter-unit cell interaction Hamiltonians H and V for the unstrained dimerized TP isomer. The parameters are in eV.

H	H_{ss}^{11}	H_{PyPy}^{11}	H_{PzPz}^{11}	H_{PxPx}^{11}	H_{ss}^{12}	H_{PyPy}^{12}	H_{PzPz}^{12}	H_{PxPx}^{12}	H_{sPy}^{12}	H_{sPx}^{12}	H_{PxPy}^{12}
	-10.426	8.747	0.288	-8.174	-2.796	-2.726	-3.188	-1.750	0.201	0.356	0.814
V	V_{ss}^{11}	V_{PyPy}^{11}	V_{PxPx}^{11}	V_{sPx}^{11}	V_{ss}^{21}	V_{PyPy}^{21}	V_{PzPz}^{21}	V_{PxPx}^{21}	V_{sPy}^{21}	V_{sPx}^{21}	V_{PxPy}^{21}
	-0.474	0.106	0.748	0.231	-2.242	-1.920	-2.421	-0.365	-1.289	2.611	-1.015

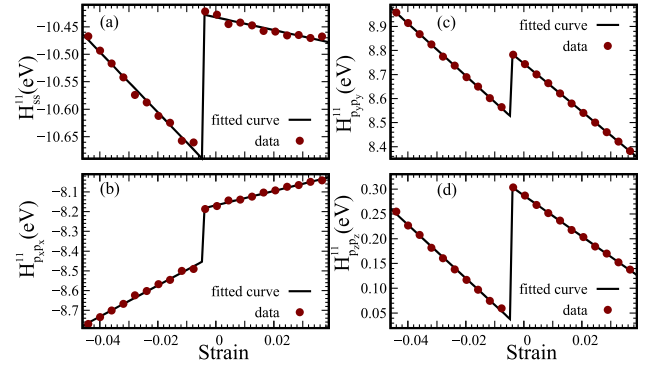
$H^{11} = H^{22}$ and two off-diagonal sub Hamiltonians which represent their interactions are conjugate transpose of each other i.e., $H^{12} = (H^{21})^\dagger$ (see figure 1(b) for H^{11} and H^{22}). Furthermore, only diagonal entries of H^{11} (i.e., H_{ss}^{11} , H_{PyPy}^{11} , H_{PzPz}^{11} and H_{PxPx}^{11}) are nonzero. Though diagonal entries of H^{12} (i.e., H_{ss}^{12} , H_{PyPy}^{12} , H_{PzPz}^{12} and H_{PxPx}^{12}) are distinct, its nonzero off-diagonal entries are related as $H_{sPy}^{12} = -H_{PyS}^{12}$, $H_{sPx}^{12} = -H_{PxS}^{12}$ and $H_{PxPy}^{12} = H_{PyPx}^{12}$. In the case of the inter-unit cell Hamiltonian, V , diagonal sub Hamiltonians which describe the interactions between the third neighbours are the same ($V^{11} = V^{22}$). Ignoring the fourth neighbours makes V^{12} a null matrix (see figure 1(b) for V^{11} , V^{12} and V^{21}). Among nonzero entries of V^{11} , only two diagonal V_{ss}^{11} and V_{PxPx}^{11} are distinct while four other entries are related as $V_{PyPy}^{11} = V_{PzPz}^{11}$ and $V_{sPx}^{11} = -V_{PxS}^{11}$. Nonzero off-diagonal entries of V^{21} are related as $V_{sPy}^{21} = -V_{PyS}^{21}$, $V_{sPx}^{21} = -V_{PxS}^{21}$ and $V_{PxPy}^{21} = V_{PyPx}^{21}$ and all its diagonal entries (i.e., V_{ss}^{21} , V_{PyPy}^{21} , V_{PzPz}^{21} and V_{PxPx}^{21}) are distinct. Considering these constraints, both Hamiltonians H and V have only eleven distinct nonzero entries which are mentioned for the unstrained dimerized TP isomer in table 2. The explicit form of the Hamiltonians are given in the supplemental material (<http://stacks.iop.org/JPhysCM/32/285401/mmedia>).³

4. Hamiltonian describing strain effects

Understanding the material responses to the mechanical interactions is crucial for their best exploitation. Strain is the measure of how much a material is stretched or deformed by a force. Cauchy strain is expressed as the ratio of the total deformation to the initial dimension of the material acted upon by the forces [64]. In one dimensional systems, it can simply be defined as the ratio of the change in the length of the material Δl to its original length l_0 as

$$\varepsilon = \frac{\Delta l}{l_0} = \frac{l - l_0}{l_0}. \quad (6)$$

This is positive if the structure is stretched and negative if it is compressed. Considering this definition, to illustrate the effects of strain on the dimerized TP isomer, the distance between two successive CH groups, a , along the molecular symmetry axis x (see figure 1(a)), is varied in 21 steps, in a way that the strain magnitude changes in the

**Figure 4.** Intra-unit cell diagonal Hamiltonian, H^{11} entries with different applied strain magnitudes ε and fitted step functions. The entries H_{ss}^{11} , H_{PxPx}^{11} , H_{PyPy}^{11} and H_{PzPz}^{11} are depicted in (a), (b), (c) and (d), respectively. The fitted functions are shown with black curves.**Table 3.** Fitting parameters a_1 , a_2 , b_1 and b_2 , for the intra-unit cell diagonal Hamiltonian different entries, the maximum of the valance band (MVb), the minimum of the conduction band (mCb) as a function of strain $f(\varepsilon) = (a_1 + b_1\varepsilon)\Theta(\varepsilon - \varepsilon_0) + (a_2 + b_2\varepsilon)\Theta(\varepsilon_0 - \varepsilon)$ and the energy gap E_g of the TP with different strain magnitudes as $f(\varepsilon) = a_1 + b_1(\varepsilon - \varepsilon_0)$.

Parameter	a_1	a_2	b_1	b_2
H_{ss}^{11}	-10.432	-10.715	-1.167	-5.486
H_{PyPy}^{11}	8.746	8.476	-9.961	-10.905
H_{PzPz}^{11}	0.287	0.012	-4.113	-5.386
H_{PxPx}^{11}	-8.168	-8.416	3.636	7.883
MVb	-0.602	-0.873	-3.996	-4.898
mCb	0.718	0.447	-5.111	-6.011
E_g	1.325	—	-1.116	—

range of $-0.044 \leq \varepsilon \leq 0.036$ which is quite far from the value $\varepsilon \simeq 1$ in which the trans polyacetylene chain is broken down by it [65, 66] to insure its applicability. In each step, the new DFT band structure is calculated, its relative TB Hamiltonian is modeled and its SK coefficients are calculated (see the supplemental material).³ Typically, effects of a short range strain on the entries of the TB Hamiltonian are modeled by a well defined differentiable function, e.g., Peierls pseudo magnetic phase. Depicting the TB Hamiltonian entries with respect to different strain magnitudes illuminates the strange behaviour in its diagrams. As it is illustrated for diagonal entries of the intra-unit cell Hamiltonian, H^{11} , in figure 4, at a certain compression strain magnitude, the diagram behaves like a step function. By nonlinear fitting of these data, a step function is fitted to these data as

³ The explicit form of both Hamiltonians H and V for the dimerized TP isomer was given in supplemental materials. Furthermore, the SK coefficients, the Hamiltonian entries and the fitting diagrams for the rest of the strained Hamiltonians can be found there.

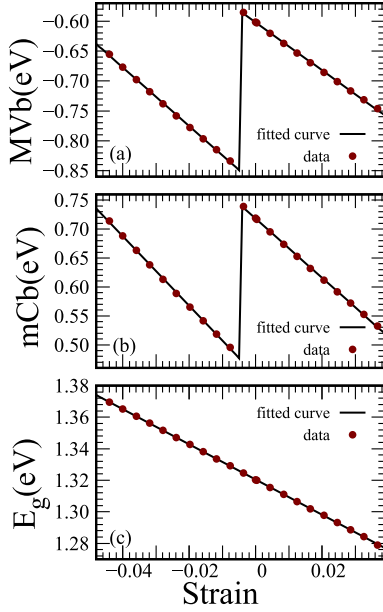


Figure 5. Maximum of the valence band (MVb) (a), the minimum of the conduction band (mCb) (b) and the energy gap of the TP (c) as a function of strain. The fitted functions are shown with black curves.

$f(\varepsilon) = (a_1 + b_1\varepsilon)\Theta(\varepsilon - \varepsilon_0) + (a_2 + b_2\varepsilon)\Theta(\varepsilon_0 - \varepsilon)$ where a_1 , a_2 , b_1 , b_2 and ε_0 are fitting parameters whose magnitudes are given in table 3 and Θ is the Heaviside step function. For the other Hamiltonian entry diagrams and their relative fitting parameters, see the supplemental material.³

Investigating the maximum of the valence band (MVb) and the minimum of the conduction band (mCb) in the band structures of the strained systems, sheds more light on this step like behaviour. In figures 5(a) and (b), these data are depicted respectively. Again, a step like behaviour is found. Their nonlinear fitting, result in a same step function with different fitting parameters which are considered in table 3. Both MVb and mCb change at the same value of the compression strain with the same magnitudes. Therefore, the energy gap of the system, is a linear function of the strain as illustrated in figure 5(c). The fitted function is a line with the equation $f(\varepsilon) = a_1 + b_1(\varepsilon - \varepsilon_0)$ whose fitting parameters a_1 and b_1 are mentioned in table 3.

Unlike all the other fitting parameters that change during the fitting procedure, one parameter remains fixed in all fitted functions which is the compression fixed point $\varepsilon_0 = -0.0046$. At this peculiar strain point, all Hamiltonian entries face with a jump in their energy (see figures 4 and 5). This movement in the energy changes the band structure of the system as shown in figure 6. In this figure, it is clarified that by compression strain, the conduction band is bent, the energy gap becomes wider and more importantly, the valence band is mixed by the other bands as highlighted by a dashed circle in figure 6(a). While in the unstrained structure, these bands are tangent (see figure 6(b)), the expansion strain splits them as shown in figure 6(c). Furthermore, the energy gap becomes narrower and the conduction band is unbent.

Changing the band structures affects many physical properties of the system, especially, its charge transport properties.

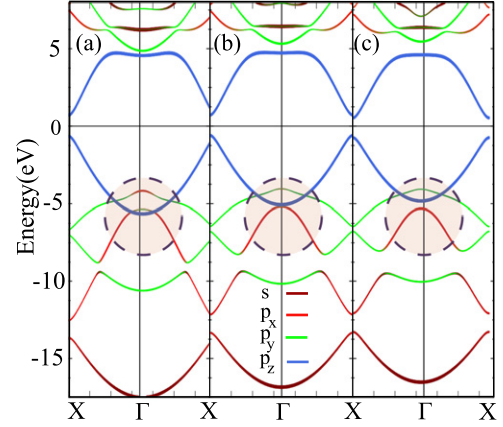


Figure 6. DFT orbital resolved band structures of TP for the compression strained structure ($\varepsilon = -0.044$) (a), the unstrained structure (b) and the expansion strained structure ($\varepsilon = 0.036$) (c). The dashed circles indicate where the band mixing and splitting take place.

Since in nanoscale systems and in ballistic regime, every band is considered as a conduction window [67], adding or removing a band opens or closes a transport window. To illustrate this, an infinite TP chain is considered as a quantum wire and its charge conductance is studied by using this new Hamiltonian. Partitioning the infinite chain to a central interaction part which is described by H_C Hamiltonian connected to two semi infinite isolated electrodes with Hamiltonians H_L and H_R which are interacting with them via $V_{LC(CR)} + V_{LC(CR)}^\dagger$ Hamiltonians (see figure 1(c)), the general Hamiltonian of the system becomes $H_S = H_C + H_R + H_L + V_{LC} + V_{LC}^\dagger + V_{CR} + V_{CR}^\dagger$. Exploiting the Green's function method in the framework of the Landauer-Büttiker formula [68] at zero temperature, the electron conductance from the left electrode to the right one, $G_{LR}(E_F)$, with the electron Fermi energy E_F , is written as

$$G_{LR}(E_F) = \frac{e^2}{h} \text{Tr}\{\Gamma_L(E_F)g_{LR}^r(E_F)\Gamma_R(E_F)g_{RL}^a(E_F)\}, \quad (7)$$

where

$$\Gamma_{L(R)}(E_F) = i\{\Sigma_{L(R)}^r(E_F) - \Sigma_{L(R)}^a(E_F)\}, \quad (8)$$

is the coupling between the central part of the system and the left (right) electrode [69]. Therefore, the central part retarded (advanced) Green's function is defined as

$$g_{LR}^r(E_F) = (g_{RL}^a(E_F))^\dagger = \frac{1}{\epsilon - H_C - \Sigma_L^r(E_F) - \Sigma_R^r(E_F)}, \quad (9)$$

where $\epsilon = E_F + i\eta$ with the phenomenological tiny broadening parameter η . The retarded self energies of electrodes are defined as

$$\Sigma_{L(R)}^r = [V_{LC(CR)}^\dagger G_{L(R)} V_{LC(CR)}] = (\Sigma_{L(R)}^a)^\dagger. \quad (10)$$

The surface Green's function of the left (right) semi infinite electrode $G_{L(R)} = [\epsilon - H_{L(R)}]^{-1}$ can numerically be determined by using an iterative method [70–72] and the density of states (DOS) is given by $\text{DOS} = -\frac{1}{\pi} \Im\{\text{Tr}[g_{LR}^r]\}$.

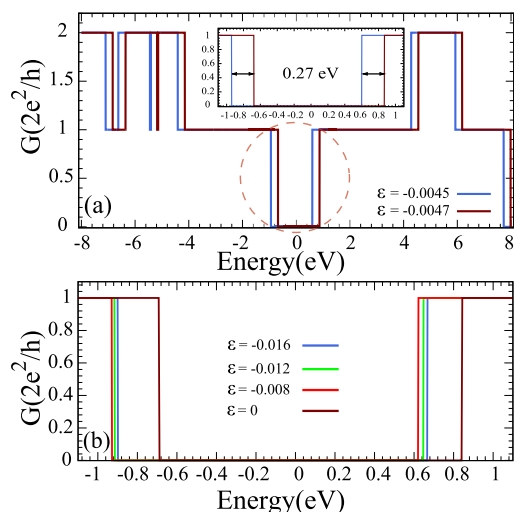


Figure 7. Electronic conductance of the dimerized TP chain under compression strain with a small value after ($\epsilon = -0.0045$) and before ($\epsilon = -0.0047$) the peculiar compression strain value (a). Charge conductance in the absence ($\epsilon = 0$) and presence of strain with different values ($\epsilon = -0.008, -0.012$ and -0.016) (b). The inset represents the magnified part of (a) indicated by dashed ellipse for illustration of the shifting in the energy.

By using the TB Hamiltonians for the strained TP, the electronic charge conductance of a TP chain with 16 carbon atoms in its central part is calculated for the strain with a small value (i.e., $\delta_0 = 10^{-4}$) before (i.e. $\epsilon_0 - \delta_0 = -0.0047$) and after (i.e. $\epsilon_0 + \delta_0 = -0.0045$) the peculiar compression strain value (i.e. $\epsilon_0 = -0.0046$) and the results are plotted in figure 7(a). The main result is that the charge conductance for strain magnitudes before and after this point, has a shift in energy whose magnitude is 0.27 eV. This is an important capability that without applying any external electric field or bias, just with compression strain the system behaves in this manner. In energies $-0.94 < E_F < -0.67$ eV ($0.59 < E_F < 0.86$ V), as magnified by inset of figure 7(a), the charge conductance is changed from one to zero (zero to one) by changing the compression strain which can work as an on/off switch for electron transport. This sudden on/off behaviour shows that the trans polyacetylene molecule can be used in straintronic devices such as strain sensors and strain switches. The energy shifting magnitude is large enough to be exploited and applied in practical devices. The conductance shifting shown in figure 7(a) is related to two closely adjacent values of compression strains. Furthermore, the charge conductance in the absence and presence of strain are investigated and their results are depicted in figure 7(b). This figure shows the charge conductance for $\epsilon = 0$ (in the absence of strain) and for different strain values ($\epsilon = -0.008, -0.012$ and -0.016) which are far from the peculiar point. It is observed that in the presence of strain, a shift for charge conductance toward the lower energy takes place. These charge conductance shifts for different strain values are similar to figure 7(a) and have considerable values for straintronic applications.

All of the above calculations for larger chains with 32 and 124 carbon atoms are repeated and it is found that the results do not change and are length independent.

At the end of this section, it is worth mentioning that the results found for straintronic properties of trans polyacetylene cannot be obtained by using the conventional SSH Hamiltonian model because it considers only two conduction and valance bands and is hassled to predict the band mixing or splitting for TP.

5. Summary and conclusions

In this paper, the linear combination of atomic orbitals method in Slater–Koster approach with fitting DFT based band structure data was used to propose a tight-binding Hamiltonian up to the third nearest neighbours for a dimerized trans polyacetylene. Furthermore, Green’s function method in combination with the Landauer–Büttiker formalism were applied to find the charge conductance and the DOS in a TP chain as a quantum wire. By changing the distance between two successive CH groups, a , along the molecular symmetry axis and remodeling the TB Hamiltonian for new structures by using the new DFT band structure data, effects of compression and expansion strain were studied. Investigating the Hamiltonian entries for different strain magnitudes, reveals a peculiar point in compression strain (i.e., $\epsilon_0 = -0.0046$), at which they are faced with a jump in their magnitude. Nonlinear fitting of the entries, despite typical models which are continuous differentiable functions based on Peierls distortion phase, results in a fitted step function for their behaviour under strain with different fitting parameters for each entry. At this peculiar compression value, the DOS accumulation suddenly moves in the energy which leads to a 0.27 eV shift in the energy for charge conductance. These features nominate the trans polyacetylene molecule as an adequate candidate for straintronic applications, specially strain sensors and strain switches.

ORCID iDs

M Ali M Keshtan  <https://orcid.org/0000-0001-7591-3427>
 Mahdi Esmailzadeh  <https://orcid.org/0000-0002-7184-2745>

References

- [1] Atanasov V and Saxena A 2011 *J. Phys.: Condens. Matter.* **23** 175301
- [2] Roy K, Bandyopadhyay S and Atulasimha J 2011 *Appl. Phys. Lett.* **99** 063108
- [3] Bukharaev A A, Zvezdin A K, Pyatakov A P and Fetisov Y K 2018 *Phys.-Usp.* **61** 1175
- [4] Si C, Sun Z and Liu F 2016 *Nanoscale* **8** 3207
- [5] Biswas A K, Atulasimha J and Bandyopadhyay S 2015 *Nanotechnology* **26** 285201
- [6] Amorima B *et al* 2016 *Phys. Rep.* **617** 1
- [7] Naumis G G, Barraza-Lopez S, Oliva-Leyva M and Terrones H 2017 *Rep. Prog. Phys.* **80** 096501
- [8] Cao Q, Geng X, Wang H, Wang P, Liu A, Lan Y and Peng Q 2018 *Crystals* **8** 357

- [9] Radchenko T M, Tatarenko V A, Lizunov V V, Molodkin V B, Golentus I E, Sahalianov I Y and Prylutsky Y I 2019 *Phys. Status Solidi B* **256** 1800406
- [10] Sahalianov I Y, Radchenko T M, Tatarenko V A, Cuniberti G and Prylutsky Y I 2019 *J. Appl. Phys.* **126** 054302
- [11] Kelley T W, Baude P F, Gerlach C, Ender D E, Muyres D, Haase M A, Vogel D E and Theiss S D 2004 *Chem. Mater.* **16** 4413
- [12] McCreery R L 2004 *Chem. Mater.* **16** 4477
- [13] Fahlman M, Fabiano S, Gueskine V, Simon D, Berggren M and Crispin X 2019 *Nat. Rev. Mater.* **4** 627
- [14] Coropceanu V, Chen X K, Wang T, Zheng Z and Brédas J L 2019 *Nat. Rev. Mater.* **4** 689
- [15] Liu H *et al* 2018 *Nat. Mater.* **17** 308
- [16] Guo L, Qin Y, Gu X, Zhu X, Zhou Q and Sun X 2019 *Front. Chem.* **7** 428
- [17] Zhou L, Mao J, Ren Y, Han S T, Roy V A L and Zhou Y 2018 *Small* **14** 1703126
- [18] Ling H, Liu S, Zheng Z and Yan F 2018 *Small* **2** 1800070
- [19] Yan T, Wang Z and Pan Z J 2018 *Curr. Opin. Solid State Mater. Sci.* **22** 213
- [20] Ge G, Huang W, Shao J and Dong X 2018 *J. Semicond.* **39** 011012
- [21] Hammock M L, Chortos A, Tee B C K, Tok J B H and Bao Z 2013 *Adv. Mater.* **25** 5997
- [22] Chou H H *et al* 2015 *Nat. Commun.* **6** 8011
- [23] Yamada T, Hayamizu Y, Yamamoto Y, Yomogida Y, Izadi-Najafabadi A, Futaba D N and Hata K 2011 *Nat. Nanotechnol.* **6** 296
- [24] Seyedin S, Zhang P, Naebe M, Wang X and Razal J M 2019 *Mater. Horiz.* **6** 219
- [25] Shirakawa H and Ikeda S 1971 *Polym. J.* **2** 231
- [26] Su W P, Schrieffer J R and Heeger A J 1979 *Phys. Rev. Lett.* **42** 1698
- Su W P, Schrieffer J R and Heeger A J 1980 *Phys. Rev. B* **22** 2099
- Su W P, Schrieffer J R and Heeger A J 1983 *Phys. Rev. B* **28** 1138
- [27] Heeger A J, Kivelson S, Schrieffer J R and Su W P 1988 *Rev. Mod. Phys.* **60** 781
- [28] MacDiarmid A G and Heeger A J 1980 *Synth. Met.* **1** 101
- [29] Conwell E M 1987 *IEEE Trans. Electr. Insul.* **22** 591
- [30] Brédas J L, Chance R R, Baughman R H and Silbey R 1982 *J. Chem. Phys.* **76** 3673
- [31] Jeyadev S and Conwell E M 1987 *Phys. Rev. Lett.* **58** 258
- Jeyadev S and Conwell E M 1988 *Phys. Rev. Lett.* **61** 361
- [32] Cao Y, Smith P and Heeger A J 1991 *Polymer* **32** 1210
- [33] Masuda T, Tang B Z, Tanaka A and Higashimura T 1986 *Macromolecules* **19** 1459
- [34] Rothberg L, Jedju T M, Etemad S and Baker G L 1986 *Phys. Rev. Lett.* **57** 3229
- [35] Glick A J and Bryant G W 1986 *Phys. Rev. B* **34** 943
- [36] Mintmire J W and White C T 1983 *Phys. Rev. B* **28** 3283
- Mintmire J W and White C T 1987 *Phys. Rev. B* **35** 4180
- [37] Paloheimo J and von Boehm J 1992 *Phys. Rev. B* **46** 4304
- [38] Suhai S 1995 *Phys. Rev. B* **51** 16553
- [39] Tuyarot D E, Koiller B and Capaz R B 2000 *Phys. Rev. B* **61** 7187
- [40] Weinberger B R, Ehrenfreund E, Pron A, Heeger A J and MacDiarmid A G 1980 *J. Chem. Phys.* **72** 4749
- [41] Vogl P and Campbell D K 1989 *Phys. Rev. Lett.* **62** 2012
- [42] Saito R and Kamimura H 1983 *J. Phys. Soc. Japan* **52** 407
- [43] Teramae H and Yamabe T 1984 *J. Chem. Phys.* **81** 3564
- [44] Peierls R E 1955 *Quantum Theory of Solids* (Clarendon: Oxford University Press) p 108
- [45] Hieu N N and Hieu N V 2014 *Phys. Status Solidi B* **251** 1614
- [46] Polyakova T B and Suris R A 1991 *Solid State Commun.* **77** 825
- [47] Moses D, Feldblum A, Ehrenfreund E and Heeger A J 1982 *Phys. Rev. B* **26** 3361
- [48] Slater J C and Koster G F 1954 *Phys. Rev.* **94** 1498
- [49] Boker S *et al* 2011 *Psychometrika* **76** 306
- [50] Jansen R W and Sankey O F 1987 *Phys. Rev. B* **36** 6520
- [51] Ozaki T 2003 *Phys. Rev. B* **67** 155108
- [52] Ozaki T and Kino H 2004 *Phys. Rev. B* **69** 195113
- Ozaki T and Kino H 2005 *Phys. Rev. B* **72** 045121
- [53] Perdew J P, Burke K and Ernzerhof M 1996 *Phys. Rev. Lett.* **77** 3865
- [54] Becke D 1988 *Phys. Rev. A* **38** 3098
- [55] Karpfen A and Petkov J 1979 *Solid State Commun.* **29** 251
- [56] Karpfen A and Höller R 1981 *Solid State Commun.* **37** 179
- [57] Papaconstantopoulos D A and Mehl M J 1981 *J. Phys.: Condens. Matter.* **15** R413
- [58] Kwiatkowski T, Olszewski S and Wierzbicki A 1977 *Int. J. Quantum Chem.* **11** 21
- [59] Goringe C M, Bowler D R and Hernandez E 1977 *Rep. Prog. Phys.* **60** 1447
- [60] Deshpande S D and Pöde R B 1988 *Am. J. Phys.* **56** 362
- [61] Kutzelnigg W 1988 *J. Mol. Struct.* **169** 403
- [62] Levenberg K 1944 *Q. Appl. Math.* **2** 164
- [63] Marquardt D W 1963 *J. Soc. Ind. Appl. Math.* **11** 431
- [64] Landau L D and Lifshitz E M 1959 *Theory of Elasticity* (Course of Theoretical Physics vol 7) (London: Pergamon)
- [65] Druy M A, Tsang C H, Brown N, Heeger A J and MacDiarmid A G 1980 *J. Polym. Sci. Polym. Phys. Ed.* **18** 429
- [66] Chien J C W 2012 *Polyacetylene: Chemistry, Physics, and Material Science* (Amsterdam: Elsevier)
- [67] Beenakker C W J and van Houten H 1991 *Solid State Phys.* **44** 1
- [68] Büttiker M and Landauer R 1982 *Phys. Rev. Lett.* **49** 1739
- Büttiker M and Landauer R 1985 *Phys. Scr.* **32** 429
- [69] Di Ventra M 2008 *Electrical Transport in Nanoscale Systems* (New York, NY: Cambridge University Press)
- [70] Caroli C, Combescot R, Nozières P and Saint-James D 1971 *J. Phys. C* **4** 916
- [71] Lopez-Sancho M, Lopez-Sancho J and Rubio J 1984 *J. Phys. F: Met. Phys.* **14** 1205
- [72] Buongiorno Nardelli M 1999 *Phys. Rev. B* **60** 7828